

Acceleration of Particles by Oblique Shocks and Cosmic Ray Spectra around the Knee Region

K. Kobayakawa ^{a,1} Y. Sato ^b T. Samura ^c

^a*Fukui University of Technology, Gakuen 3-6-1, Fukui, Fukui, 910-8505, Japan*

^b*School of Science, Kwansei Gakuin University, 1-1-155, Uegahara, Nishinomiya,
Hyogo, 662-8501, Japan*

^c*Department of Electrical and Computer Engineering, Akashi National College of
Technology, 679-3, Nishioka, Uozumi-cho, Akashi, 674-8501, Japan*

Abstract

We consider the first order Fermi acceleration on the presumption that the shock fronts around supernova remnants cross outer magnetic fields with various angles. These oblique shocks concerned with, accelerate particles more efficiently than parallel shocks and elevate the achievable maximum energies. The primary cosmic ray spectrum is strongly dependent upon these energies. When indices and absolute fluxes at 10^{12} eV are given for several nuclear groups from experimental data, the total primary spectrum shows a smooth knee behavior at $\sim 10^{15}$ eV and fits the flux data well up to several times of 10^{17} eV. It is also shown that the chemical composition changes significantly from lighter to heavier nuclei as energies of particles exceed the knee. It is compared with data, too.

Key words: PACS 96. 40. De, 96. 50. Fm, 98. 70. Sa. Cosmic rays, Fermi acceleration, Oblique shock waves, Energy spectrum, Composition.

¹ Corresponding author: Email: kobayakw@ccmails.fukui-ut.ac.jp

1 Introduction

For the past several years, many measurements of the primary spectrum of cosmic rays and their chemical composition have been performed. Some of them are direct measurements by balloon-borne experiments up to about 100 TeV. Others are by indirect ground-based experiments. These experiments have investigations of so-called knee as one of their main aims. Recent reports say that the all-particle spectrum of cosmic rays presents not a sudden steepening, but a gradual bent near the energy of knee, $E_{\text{knee}} = (2 \sim 4) \times 10^{15}$ eV, from $E^{-(2.6 \sim 2.8)}$ to $E^{-(3.0 \sim 3.2)}$ [1]. This value of E_{knee} lessens about a half from earlier reports [2]. The chemical composition of cosmic rays below E_{knee} is directly measured and shows almost constant in term of the average mass number expressed by $\langle \ln A \rangle$. However, data of $\langle \ln A \rangle$ above E_{knee} fairly scatter because of indirect air shower observations. It is also noted that values of $\langle \ln A \rangle$ is significantly affected by hadronic interaction models included in simulations of extensive air showers [3].

There is a common consensus, on the other hand, that particles in the energy range up to E_{knee} are considered to be accelerated efficiently by shock waves around supernova remnants as follows. When particles cross the shock front to and fro frequently, they obtain large energies proportional to the shock velocity, i.e. the first order Fermi acceleration (for review, see [4]). This stochastic acceleration and a deformation of source spectra due to energy dependent diffusion from the galaxy can explain power-law spectrum up to the knee. The scenario leads that the maximum energy E_{max} , that particles can be achieved with shock acceleration mechanism, is expected to nearly equal E_{knee} .

Actually the E_{max} is estimated to $\sim 3Z \times 10^{13}$ eV [5], where Z is an atomic number, which is much lower than E_{knee} . However, this value is achieved by parallel shock acceleration where the normal of shock front is parallel to the direction of outer magnetic field. That is not the case for non-parallel, where the angle α_1 between the shock normal and the field direction is not zero. These oblique shocks can accelerate particles much more efficiently. For extremely oblique shocks, E_{max} is raised by a couple of orders than parallel cases. The detail will be described in the next section.

In this paper we attempt to explain the knee behavior of energy spectrum with the acceleration mechanism by oblique shocks. Our model is based on a simple idea as follows [6]. After a supernova explosion, a shock wave is formed around its remnant and expands freely into the interstellar medium. The shape of the shock front is then supposed to be almost spherically symmetric. The directions of the interstellar magnetic field over a wide range will be nearly at random rather than well aligned. It is therefore assumed that the field lines meet the shock front with a random α_1 and the cosine of α_1 distributes

uniformly. Since E_{\max} are strongly dependent upon α_1 , particles will get a wide range of energies even around E_{knee} . This leads to the slow change of spectral index for each elemental group. So, the total flux, the sum of groups, shows a gradual change around the knee. We choose the spectral indices and absolute fluxes for several nuclear groups at 1 TeV as initial conditions. Then, following to our model, we calculate energy spectra up to 10^6 TeV for several nuclear families from which the total spectrum and the energy dependence of chemical composition can be directly obtained. These results are compared with recent data of balloon and air shower experiments.

2 Acceleration mechanism by oblique shocks

In this section we will review the particle acceleration process by oblique shocks in detail, following Ostrowski [7]. Some misprints contained in the original paper are also corrected. In an oblique shock, particles are not only transmitted by its front but reflected by it. Because the energies of particles are raised by both of these interactions, the acceleration by oblique shocks is more efficient than that by parallel ones.

The energy of a cosmic ray particle is conserved during the interaction with the shock front if the amplitudes of magnetic field fluctuations are sufficiently small compared with the average field. Upstream and downstream parameters are denoted by subscripts 1 and 2, respectively. The symbols of \parallel and \perp stand for the parallel and normal components to magnetic field lines, respectively. Suffix “n” means the component perpendicular to the shock front. In oblique shocks, variables with the suffix “ \parallel ” discriminate from those with “n”. A unit of light velocity $c = 1$ is used in this section unless otherwise specified.

2.1 Particle interactions with the shock front

Suppose a plane shock wave whose front is propagating at a non-relativistic speed U_1 with respect to the upstream medium. The shock normal crosses magnetic field lines B_1 at an angle α_1 in the upstream. A schematic view in the upstream rest frame is shown in Fig. 1. Parameters of downstream in its rest frame, magnetic field inclination β_2 and shock velocity U_2 can be expressed by upstream ones [8].

Let us consider a particle penetrating the shock front. The particle velocity in the downstream parallel to B_2 is described by

$$v_{2\parallel} = \sqrt{1 - \frac{B_2}{B_1} \sin^2 \theta} v_1, \quad (1)$$

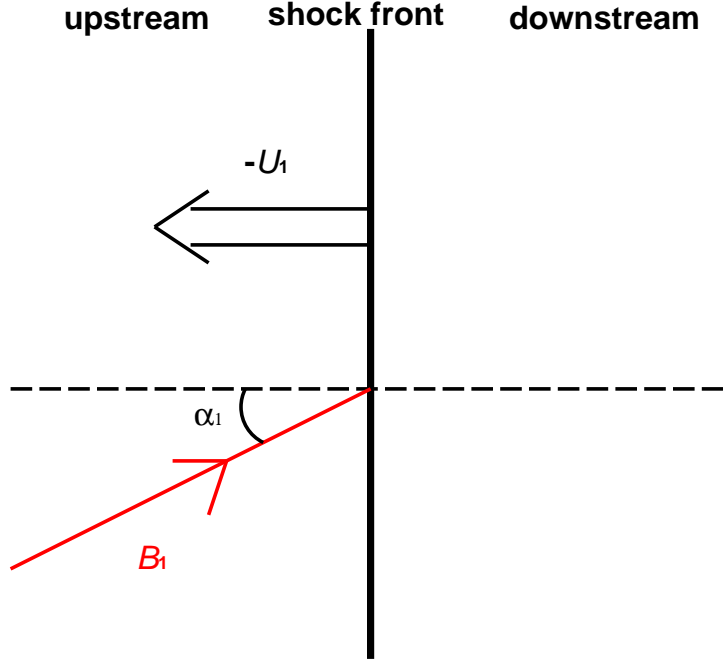


Fig. 1. The schematic diagram of an oblique shock where the outer magnetic field B_1 intersects the normal of the shock front with non-zero angle α_1 .

where v_1 is the particle velocity in the upstream and θ is the pitch angle of gyration. Since $B_2 > B_1$, there is an angle that satisfies $v_{2\parallel} = 0$. When angles are larger than this critical value, particles are reflected by the shock front due to the effect of magnetic mirroring. Defining μ as the cosine of pitch angle, the conditions of reflection or penetration can be easily written.

In order to study the particle interaction with the velocity jump at the shock surface, we first transform the system from the plasma rest frame to de-Hoffmann-Teller frame [9] (abbreviate the H-T frame, hereafter). In the H-T frame, electric fields vanish globally and hence, the energy of a particle does not change before and after interactions. Assuming that the magnetic moment of a particle is conserved, one can easily derive the results of interactions. Finally, all variables should be transformed back into the respective plasma rest frame.

- (i) For particles reflected by the shock front (denoted by the subscript 'r')
From eq. (1), particles are reflected by the shock front when $0 < \mu < \mu_0$, in the H-T frame. Here μ_0 is defined by

$$\mu_0 = \sqrt{1 - \frac{B_1}{B_2}}. \quad (2)$$

This condition transforms as $\mu_1 < \mu < \mu_2$, where $\mu_1 \equiv -V_1$,

$\mu_2 \equiv (\mu_0 - V_1)/(1 - \mu_0 V_1)$ and $V_1 = U_1/\cos \alpha_1$ in the upstream rest frame. A particle with an energy E will be changed into E_r after the reflection, the ratio is

$$\frac{E_r}{E} = \gamma_1^2(1 + V_1^2 + 2V_1\mu), \quad (3)$$

where $\gamma_1 = (1 - V_1^2)^{-1/2}$.

(ii) For upstream particles transmitted downstream ('12')

If $\mu > \mu_0$, particles are transmitted downstream. Transforming back this range to the upstream rest frame, one obtain $\mu > \mu_2$. The ratio of the energy after to before the transmission is

$$\frac{E_{12}}{E} = \gamma_1 \gamma_2 [1 + V_1 \mu - V_2 \sqrt{(1 + V_1 \mu)^2 - (1 - \mu^2)/(1 - \mu_0^2)/\gamma_1^2}], \quad (4)$$

where $V_2 = U_2/\cos \beta_2$ and $\gamma_2 = (1 - V_2^2)^{-1/2}$.

(iii) For downstream particles transmitted upstream ('21')

Particles are transmitted upstream if $\mu < \mu_3$ in the downstream rest frame, where $\mu_3 \equiv -V_2$. The energy increasing rate of this process is

$$\frac{E_{21}}{E} = \gamma_1 \gamma_2 [1 + V_2 \mu - V_1 \sqrt{(1 + V_2 \mu)^2 - (1 - \mu^2)(1 - \mu_0^2)/\gamma_2^2}]. \quad (5)$$

2.2 Diffusive acceleration process

Let us assume that particles approaching the shock front are distributed almost isotropically in the plasma rest frame. In order to derive the mean energy gains and the probabilities of transmission and reflection, we use a normal component of flux density of particles approaching the shock as a weight function S_σ , where the subscript $\sigma = 'r'$ (reflection), '12' (transmission downstream), '21' (transmission upstream). Following Drury [10], we calculate the flux densities of these processes up to the first order of the fluid velocity. S_σ is measured by the normal component of the particle guiding center velocity V_{rel} and defined by $S_\sigma \equiv \int V_{\text{rel}} d\mu$. The flux density of particles by reflection is calculated from the definition,

$$S_r \equiv \int_{\mu_1}^{\mu_2} \frac{\mu \cos \alpha_1 + U_1}{1 + \mu \cos \alpha_1 U_1} d\mu \simeq \frac{1}{2} \mu_0^2 \cos \alpha_1. \quad (6)$$

In the same way the flux density of particles transmitted downstream is

$$S_{12} \equiv \int_{\mu_2}^1 \frac{\mu \cos \beta_2 - U_2}{1 - \mu \cos \beta_2 U_2} d\mu \simeq \frac{1}{2} (1 - \mu_0^2) \cos \alpha_1. \quad (7)$$

Therefore, the probabilities of reflection and transmission of particles in upstream are respectively

$$P_r = \frac{S_r}{S_r + S_{12}} \simeq \mu_0^2, \quad P_{12} = \frac{S_{12}}{S_r + S_{12}} \simeq 1 - \mu_0^2, \quad (8)$$

where $P_r + P_{12} = 1$. The energy gain of a particle per each interaction (reflection and transmission) is calculated from the definition respectively,

$$d_r \equiv \frac{1}{S_r} \int_{\mu_1}^{\mu_2} V_{\text{rel}} \left(\frac{E_r}{E} - 1 \right) d\mu = \frac{4}{3} V_1 \mu_0. \quad (9)$$

$$d_{12} \equiv \frac{1}{S_{12}} \int_{\mu_2}^1 V_{\text{rel}} \left(\frac{E_{12}}{E} - 1 \right) d\mu = \frac{2}{3} \left(\frac{1 - \mu_0^3}{1 - \mu_0^2} V_1 - V_2 \right). \quad (10)$$

These expressions are valid up to the first order of fluid velocities and $d_{21} = d_{12}$. Using eqs. (8) -(10), we obtain the mean energy gain of particles

$$d \equiv P_r d_r + P_{12} d_{12} + P_{12} P_{21} d_{21} = \frac{4}{3} V_1 - \frac{4}{3} V_2 (1 - \mu_0^2). \quad (11)$$

This is the well-known first order Fermi acceleration mechanism. In the previous estimation, the probability that downstream particles will escape from the shock is neglected, and hence $P_{21} = 1$.

2.3 Characteristic acceleration time

The characteristic acceleration time, t_{acc} , is defined by the energy E divided by the rate of its change due to the acceleration process such as

$$t_{\text{acc}} = \frac{E}{\Delta E / \Delta t} = \frac{\Delta t}{d}. \quad (12)$$

Here Δt is the average time interval between successive interactions and given as

$$\Delta t = t_1 P_r + t_1 P_{12} + t_2 P_{12} P_{21} = t_1 + P_{12} t_2, \quad (13)$$

where t_1 and t_2 are mean residence times in upstream and downstream, respectively. Both t_1 and t_2 are expressed in terms of the normal component to the shock front of the diffusion coefficient, κ_n ,

$$\kappa_{ni} = \kappa_{\parallel i} \cos^2 \psi_i + \kappa_{\perp i} \sin^2 \psi_i, \quad (14)$$

where $i = 1$ (upstream) or 2 (downstream); $\psi_1 = \alpha_1$, $\psi_2 = \beta_2$. In the limit of the one-dimensional diffusion coefficient ($\kappa_{\parallel} \gg \kappa_{\perp}$), κ_n is expressed by mean free path of a particle perpendicular to the shock front, ℓ_n ;

$$\kappa_n = \frac{1}{2} \ell_n v_n. \quad (15)$$

If the spatial part of a source is distributed homogeneously on the surface at the distance ℓ from the shock, t_i are obtained when $\ell_n = \ell$,

$$t_i = \frac{\ell_{ni}}{U_i} = \frac{2\kappa_{ni}}{v_{ni} U_i}. \quad (16)$$

The parallel and normal components of the diffusion coefficient can be written with parameter x ,

$$\kappa_{\parallel i} = \kappa_{Bi} x_i, \quad \kappa_{\perp i} = \frac{\kappa_{Bi}}{x_i}, \quad (17)$$

where the value of x is of the order of inverse square of field fluctuations $(\frac{B}{\delta B})^2$. The Bohm diffusion coefficient, κ_B , is given by

$$\kappa_{Bi} = \frac{1}{3} r_{Li} v = \frac{Ec}{3ZeB_i}, \quad (18)$$

where r_L and Ze is the Larmor radius and electric charge of a particle, respectively. Substituting eqs. (14) and (17) into eq. (16), we obtain

$$t_i = \frac{2\kappa_{Bi}}{v_{ni} U_i} (x_i \cos^2 \psi_i + \frac{1}{x_i} \sin^2 \psi_i). \quad (19)$$

Using eqs. (11) and (19), we can easily calculate the characteristic acceleration time. Following Ostrowski [7] and Takahara [11], t_{acc} can be expressed by upstream parameters only

$$t_{acc} = \frac{3r}{U_1^2(r-1)} \kappa_B x \left[\cos^2 \alpha_1 + \frac{\sin^2 \alpha_1}{x^2} + \frac{r(\cos^2 \alpha_1 + \frac{r^2}{x^2} \sin^2 \alpha_1)}{(\cos^2 \alpha_1 + r^2 \sin^2 \alpha_1)^{\frac{3}{2}}} \right], \quad (20)$$

where r denotes the compression ratio of the shock, i.e. $r = U_1/U_2$.

2.4 The maximum energy

In order to derive the maximum energy that particles can obtain with this mechanism, we should consider the causes to restrict the acceleration. There are three main causes of restriction such as leakage from the galaxy, energy losses of particles, and the lifetime of a shock. First, subject to the leakage, the characteristic escape time from the galaxy τ_{esc} has been inferred as the order of 10^7 yr from various observations [12] and it is long for particles enough to reach high energies. Next, particles are considered to lose energy by the processes such as ionization losses, bremsstrahlung, and so on. In particular, ionization losses are significant in low energy region. The acceleration time, however, is so short that particles have been achieved to sufficiently high energies before they lose. Thus, the particle acceleration is supposed to be continued until the shock vanishes. The lifetime of the shock t_{sh} defined by R_{sh}/U_1 is estimated to hundred years. So, putting $t_{\text{acc}} = t_{\text{sh}}$ after Lagage & Cesarsky [13], we can write down the E_{max} ,

$$E_{\text{max}} = \frac{R_{\text{sh}}(r-1)}{rcx} U_1 e B_1 Z \left[\cos^2 \alpha_1 + \frac{\sin^2 \alpha_1}{x^2} + \frac{r(\cos^2 \alpha_1 + \frac{r^2}{x^2} \sin^2 \alpha_1)}{(\cos^2 \alpha_1 + r^2 \sin^2 \alpha_1)^{\frac{3}{2}}} \right]^{-1}. \quad (21)$$

Substituting the various constants for corresponding typical values and defining $\eta \equiv \cos \alpha_1$, we get E_{max} as a function of η and x ,

$$E_{\text{max}} = 2.5 \times 10^{16} [\text{eV}] \left(\frac{B_1}{30 \mu\text{G}} \right) \left(\frac{R_{\text{sh}}}{3 \text{pc}} \right) \left(\frac{U_1}{10^7 \text{m/s}} \right) \times \frac{Z}{x} \frac{r-1}{r} \left\{ \eta^2 + \frac{1-\eta^2}{x^2} + \frac{r[\eta^2 + \frac{r^2}{x^2}(1-\eta^2)]}{[\eta^2 + r^2(1-\eta^2)]^{\frac{3}{2}}} \right\}^{-1}. \quad (22)$$

Here we obtain the numerical value 2.5×10^{16} according to the recent papers. Namely, due to non-linear effects, $80/9$ times larger than ordinary values [14]. B_1 is also taken rather larger value [15,16] than the usual field strength of interstellar magnetic field.

Substituting B_1 , R_{sh} , U_1 and x for typical values in eq. (22), we obtain E_{max} as a function of $\cos \alpha_1$ and x . Figure 2 shows η dependence of E_{max} for $Z = 1$: proton, with $x = 10$, 30 , and 100 , since the value of x is considered to lie between 10 and 100 . From eq. (22), the value of E_{max} should be multiplied by Z for the nucleus with Z . As shown in Fig. 2, the E_{max} is dependent strongly

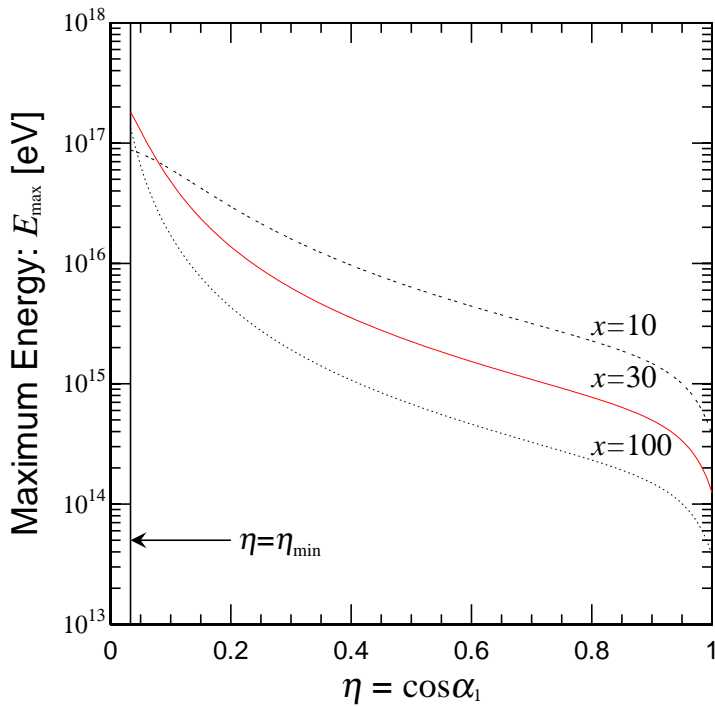


Fig. 2. The maximum energy E_{\max} for a proton with three values of x versus magnetic field inclination η . α_1 is an angle between the magnetic field and the normal of the shock front. The E_{\max} at $\eta = 1$ and $\eta = \eta_{\min}$, are the energies obtained by parallel shock and quasi-perpendicular shock acceleration, respectively. For the nucleus with the atomic number Z , E_{\max} should be multiplied by Z .

on η . The E_{\max} in quasi-perpendicular shocks is larger than in parallel shocks by two or three orders of magnitudes for each value of x .

3 Results

3.1 Our model

Based on the result that the angular dependence of the maximum energy is quite significant, we propose a simple model. In our model the shape of a shock around a supernova remnant is almost spherically symmetric and magnetic field lines intersect the shock normal with various angles. So, a uniform distribution of η is assumed. Here we do not consider the possibility that magnetic field lines tend to be perpendicular to the shock front because of Rayleigh-Taylor instabilities [17]. The value of η is restricted within the range

between η_{\min} and 1 to satisfy the condition that the shock front should not move beyond light in the H-T frame. The probability in the width $d\eta$ is then

$$f(\eta)d\eta = \frac{d\eta}{1 - \eta_{\min}} \quad (\eta_{\min} \leq \eta \leq 1), \quad (23)$$

where $\eta_{\min} = \frac{U_1}{c} \sim \frac{1}{30}$ and $(1 - \eta_{\min})^{-1}$ is the normalization factor. The range where $0 \leq \eta < \eta_{\min}$ is neglected because it occupies only 1/30 of the whole η , and is regarded as negligible. The energy achieved with the parallel shock acceleration ($\eta = 1$) is denoted by E_{critical} . Let an energy of a particle to be ε which satisfies $E_{\text{critical}} \leq \varepsilon \leq E_{\max}(\eta_{\min})$. One η corresponds to ε since $E_{\max}(\eta)$ is a monotonic decreasing function of η as shown in Fig. 2. Then the oblique shocks only with the range from η to η_{\min} can serve to give ε . Therefore, flux at ε should be multiplied by the factor $(\eta - \eta_{\min})/(1 - \eta_{\min})$. This factor may cause to make the index of the spectrum smooth change above the E_{critical} . While energies of particles are lower than E_{critical} , the spectral index remains constant.

Using the first order Fermi acceleration mechanism, we can derive the power-law energy spectrum. In the case of oblique shocks, we also expect the same power of differential spectrum dJ/dE as the parallel ones, if we take up to the terms of $O(V_1)$ and $O(V_2)$ into account. That is to say,

$$\frac{dJ}{dE} \propto E^{-p} \quad \left(\text{with} \quad p = \frac{r+2}{r-1} \right). \quad (24)$$

As for a strong shock $r = 4$, $p = 2$, which is independent of η , of course. This index is expected to be changed into $-\gamma$ (somewhat steeper) in consideration of energy dependent leakage from the galaxy [18]. We do not enter into detail discussion of this change, even though different changes are used for nuclear groups in the next subsection.

In summary, the differential energy spectra can be expressed as:

$$\begin{aligned} \frac{dJ}{dE} &= CE^{-\gamma} & (E < E_{\text{critical}}) \\ &= CE^{-\gamma} \frac{\eta - \eta_{\min}}{1 - \eta_{\min}} & (E_{\text{critical}} \leq E \leq E_{\max}(\eta_{\min})) \\ &= 0 & (E_{\max}(\eta_{\min}) < E), \end{aligned} \quad (25)$$

where C is a constant. The eq. (25) means that the curve of the flux is differentiable and changes from linear to smoothly bend above E_{critical} in a log-log diagram.

Table 1

Two choices of initial conditions at 1 TeV for the absolute value Ψ and index β in the form of eq. (26). Ψ is in the unit of $[\text{GeV}^{1.5} \text{m}^{-2} \text{s}^{-1} \text{sr}^{-1}]$.

| Elements | Z | A | Ψ_{HEGRA} | β_{HEGRA} | Ψ_{Ours} | β_{Ours} |
|----------|------|------|-----------------------|------------------------|----------------------|-----------------------|
| p | 1.0 | 1.0 | 3447 | 0.25 | 3000 | 0.27 |
| He | 2.0 | 4.0 | 2087 | 0.12 | 2200 | 0.22 |
| CNO | 7.26 | 14.5 | 885 | 0.17 | 1030 | 0.07 |
| Middle | 12.8 | 25.8 | 692 | 0.11 | 630 | 0.07 |
| sub-Fe | 21.0 | 45.0 | 99 | 0.11 | 90 | 0.07 |
| Fe | 26.0 | 55.9 | 790 | 0.11 | 720 | 0.0 |
| total | | | 8000 | | 7670 | |

When $0 \leq \eta < \eta_{\min}$, the velocity of the shock front becomes superluminal in the H-T frame although we have neglected this range in the previous discussion. If particles are accelerated effectively by some other mechanism, however, we should take this range into consideration.

3.2 The energy spectra of primary cosmic ray components

We calculate differential fluxes of various mass groups. Fluxes are multiplied by $E^{2.5}$ in order to clarify the change of spectral indices. Our flux for each chemical component is normalized to the experimental data at $E = 1$ TeV, where E is total (mass plus kinetic energy) per particle:

$$\Psi = \left[E^{2.5} \frac{dJ}{dE} \right]_{E=1\text{TeV}} = \phi E^{-\beta}, \quad (26)$$

where $\beta = \gamma - 2.5$. Here we take two different types of values of Ψ and β shown in Table 1 as initial conditions. Parameters with subscript “HEGRA” are referred from the analysis for HEGRA air shower experiment [19] and slightly modified. The values with suffix “Ours” are determined so as to fit with various experimental data around $E = 1$ TeV. We do not enter the detail why some different values of Ψ and β are taken for groups of elements such as Table 1. The most notable difference of these two models is the index β of Fe. The resultant all-particle spectrum with “HEGRA” parameters shows a more rapid fall down in high energies. For simplicity, we fix the value of x about at its geometrical mean, $x = 30$ in calculation of eq. (21).

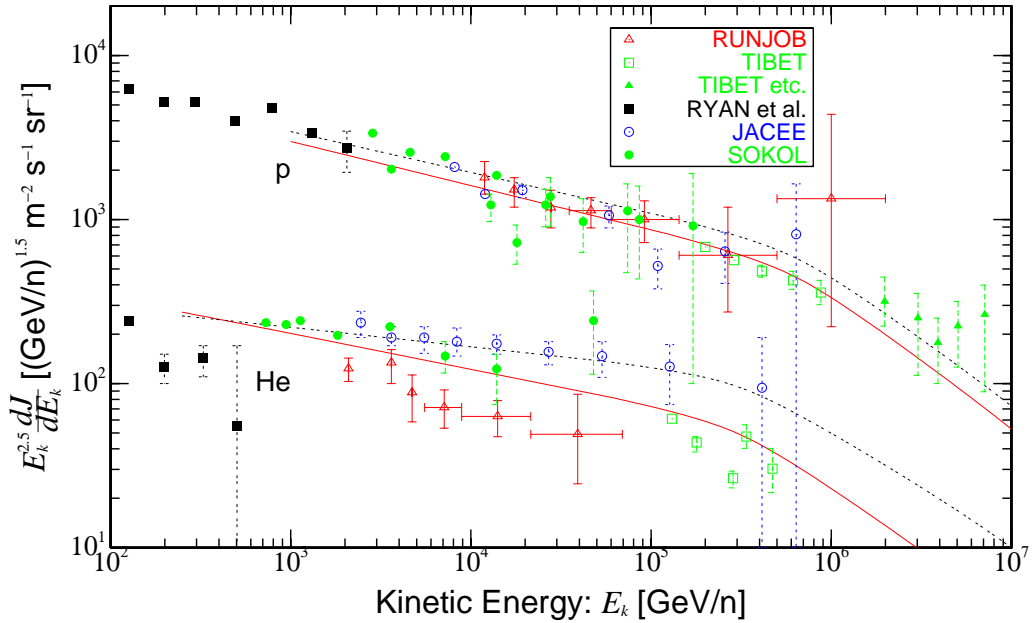


Fig. 3. Comparison of calculated fluxes of p and He with experimental data. The horizontal axis is measured in kinetic energy per nucleon (GeV/n). The solid and dashed curves represent Ours and HEGRA choices of parameters, respectively as shown in Table 1. The referred data are RUNJOB [23], Tibet γ [21], Tibet γ etc. [20] and for others see ref. [23].

In Fig. 3 we plot the calculated spectra of p and He against the kinetic energy E_k per nucleon. The theoretical spectrum with “Ours” parameters is expressed by a solid curve and that “HEGRA” parameters by a dashed ones. The energy spectrum of p starts to bend due to the η factor in eq. (25) at the energy: $E_{k,\text{critical}}(p) \simeq 1.25 \times 10^5$ GeV/n. This steepening of spectral index shows a remarkable coincidence with the recent data of Tibet air shower experiment [21]. For He, $E_{k,\text{critical}}(\text{He}) = Z(\text{He})/A(\text{He}) \times E_{\text{critical}}(p) - m_p \simeq 6.3 \times 10^4$ GeV/n. JACEE data [22] seem to show consistently this $E_{k,\text{critical}}(\text{He})$, while RUNJOB’s flux [23] somewhat lower but their highest E_k does not reach $E_{k,\text{critical}}(\text{He})$.

We also present spectra of CNO, middle, and Fe-group in Fig. 4. The “middle” corresponds to NeMgSi-group and Fe-group to our “sub-Fe” plus “Fe” in Table 1. The two curves mean the same as in Fig. 3. Fluxes of middle and those of Fe-group are reduced to $\frac{1}{10}$ and $\frac{1}{100}$ of the original value, respectively. The slow changes of spectral indices of these particles above $E_{k,\text{critical}} \simeq 6.3 \times 10^4$ GeV/n is not clearly seen from data, because direct observations are hard to take such data. Data of RUNJOB experiment are also slightly lower in this graph.

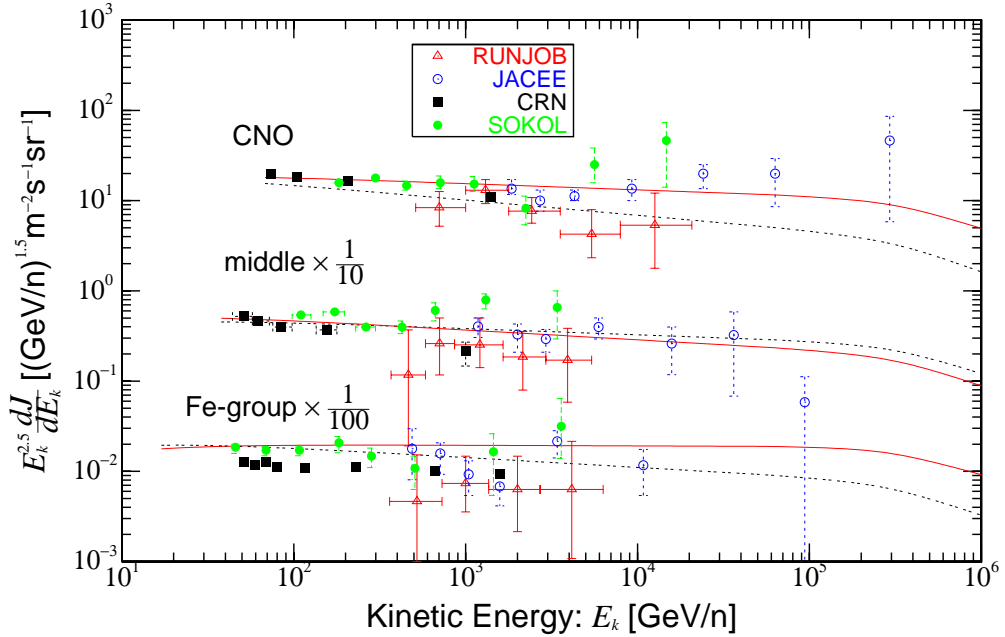


Fig. 4. Comparison of calculated fluxes of CNO-, middle, and Fe-groups with experimental data. The original fluxes of middle and of Fe-group are multiplied by 1/10 and 1/100, respectively. The solid and dashed curves mean the same as in Fig. 3. Experimental data are taken from RUNJOB's compilation [23].

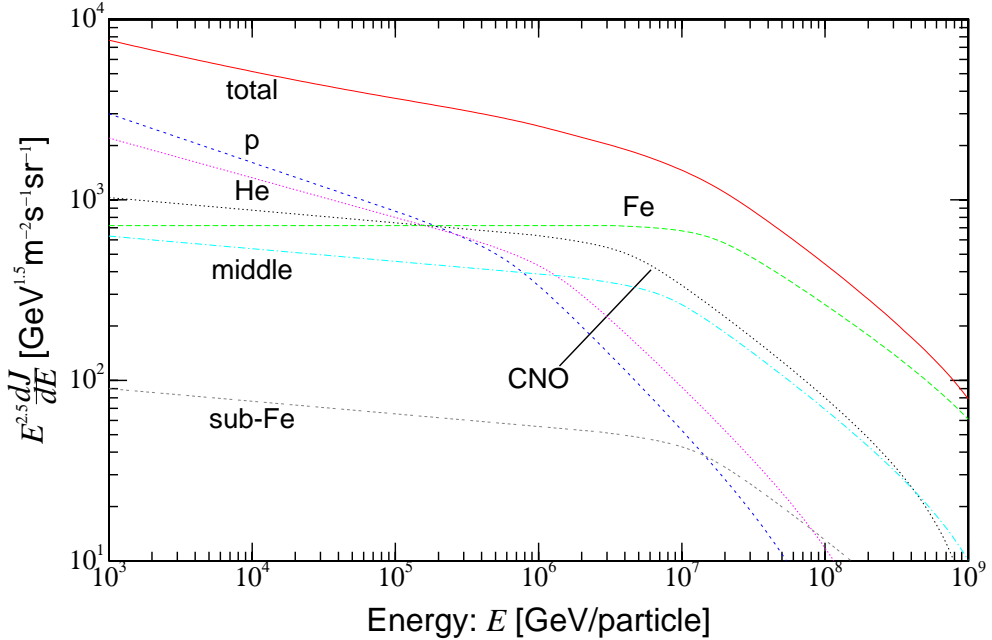


Fig. 5. The predicted fluxes of total, proton, He, and nuclear groups in the case of “Ours” parameter choices shown in Table 1.

We plot theoretical curves of spectra for various nuclear groups with Ours choice of parameters versus the whole energy per particle in Fig. 5. One can

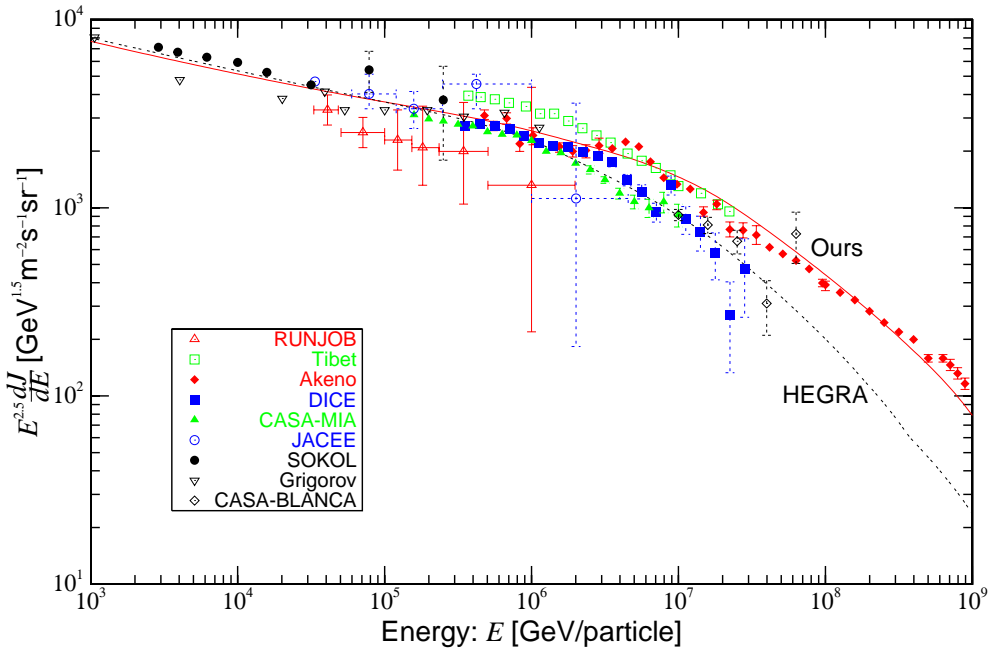


Fig. 6. Comparison of all-particle spectrum versus total energy per particle between experimental data from various groups and the present calculation. The solid and dashed curves represent the same as in Fig. 3. The data are Tibet γ [20], AKENO [2,26], DICE [27,28], CASA-MIA [29] and CASA-BLANCA [3] (here only five data points with higher energies are cited in order to avoid overcrowding since other 16 points of lower energies are almost overlap with CASA-MIA data). Others are cited from RUNJOURB's compilation [23].

see that the spectrum of lighter nuclei starts to bend at lower energies. This is just due to eqs. (22) and (25). Namely the changes occur at a fixed rigidity 1.25×10^5 GV. Summing the fluxes of all these groups, we obtain the flux of all particles and plot it also in this figure. Since the flux of each group is a smooth (differentiable) curve as mentioned above, the total flux should be smooth. The knee behavior in our model come from the η -dependence of E_{\max} due to the oblique shock acceleration expressed in eq. (25). This is different from HEGRA analysis [24], Biermann [17] and Stanev et al. [25]. In the former paper, the knee is explained by introducing breaks of slope at a fixed rigidity. The authors of latter two papers, interpret the knee as the superposition of sources from different phases of SNRs.

In Fig. 6 the two present curves of the total flux, i. e. with Ours (the same as in Fig. 5) and HEGRA choices of parameters, are compared with experimental data. As seen in this figure, Ours curve is fitted closely with Tibet γ and Akeno data [26] up to several times 10^8 GeV. While the curve with HEGRA parameters is in good agreement with DICE and CASA-MIA [29], in which both E and Ψ are about 30% lower than the Akeno data. Anyway, the total

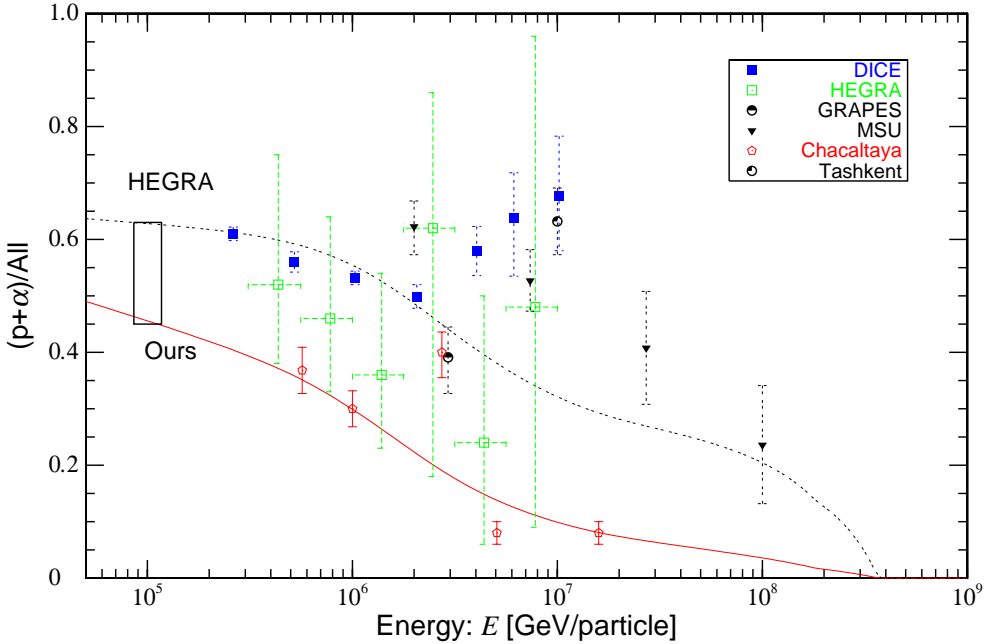


Fig. 7. Energy dependence of $(p + \alpha)/\text{All}$. Two predicted curves come from two choices of parameters as well as in Fig. 3. Experimental data are as follows: HEGRA [30], DICE [27], and others are Watson's compilation [31]. A large rectangle area shows direct measurement.

flux can be explained at least up to 10^8 GeV by our model.

The two curves in Fig. 6 are tried to be expressed in single power laws below and above E_{knee} by the least square method. For HEGRA and Ours choices $\gamma = 2.749 \pm 0.009$ and 2.670 ± 0.004 , respectively between 10^5 GeV and 3×10^6 GeV; $\gamma = 3.081 \pm 0.012$ and 2.943 ± 0.013 , respectively between 3×10^6 and 10^8 GeV. These values depend on the adopted energy range, but are compared with experimental data. For example, 2.60 ± 0.04 below and 3.00 ± 0.05 above E_{knee} from Tibet γ [1]. The corresponding values from CASA-BLANCA [3] are 2.72 ± 0.02 and 2.95 ± 0.02 .

3.3 The energy dependence of chemical composition

Using the results of energy fluxes, we examine how the chemical composition of cosmic ray particles changes with energy. The flux ratio of p plus He to all particles is plotted against the energy per particle in Fig. 7. It is shown that light components of the primary are abundant in low energy region. The theoretical curve with HEGRA parameters lies within the uncertainties of experiments quoted here. The rate of light elements, however, tends to increase again beyond the energy of several times 10^6 GeV from experiments

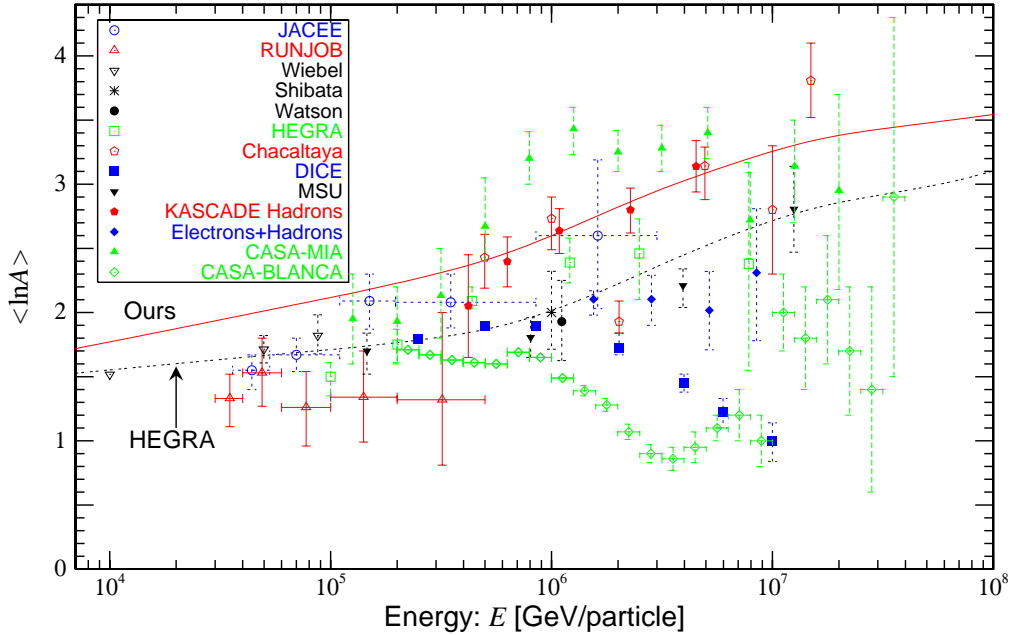


Fig. 8. Energy dependence of chemical composition of primary cosmic rays in term of $\langle \ln A \rangle$. The solid and dashed curves come from Ours and HEGRA choices of parameters, respectively as shown in Table 1. Experimental data are as follows: JACEE [22], RUNJOB [23], DICE [27] (X_{\max} +Muon), CASA-MIA [32], CASA-BLANCA (by QGSJET interaction model) [3], and others are KASCADE's compilation [33], where KASCADE's data in itself are cited of "Hadrons", and of "Electrons+Hadrons, Bayes-Classifier". The "Hadrons" alone seems to yield a too heavy composition. Chacaltaya value at 10^7 GeV is recent one [34].

of DICE and HEGRA.

As a useful indicator of the composition, we take up the average value of the logarithm of mass number A , such as

$$\langle \ln A \rangle \equiv \frac{\sum_i f_i (\ln A_i)}{\sum_i f_i}, \quad (27)$$

where f_i is the flux of i which denotes the species of each elemental group shown in Table 1. Our two $\langle \ln A \rangle$ curves versus energy E are shown and compared with various data in Fig. 8. Both curves monotonically increase with energy which are naturally led by the present model. The HEGRA gives lower values than Ours.

In Fig. 7 experimental data scatter and have large uncertainties especially above the knee. The similar trend exhibits in Fig. 8. This is due to that

ground-based measurements are indirect to study the composition. The values of $\langle \ln A \rangle$ significantly depend on experimental observables to be treated and on hadronic interaction models to be used in simulation processes. The fairly different values are reported by various groups. Some authors [27] say that $\langle \ln A \rangle$ is decreasing in energy regions larger than the knee. Other authors [3] show that $\langle \ln A \rangle$ has even a dip near E_{knee} . Almost of the rest data present that $\langle \ln A \rangle$ increases with E . So, in the present stage we can not reach a definite conclusion whether our curves are in good agreement with data or not.

4 Concluding remarks

We consider the acceleration by oblique shocks in which outer magnetic fields cross the shock normal with any angle α_1 . We calculate E_{max} as a function of $\eta = \cos \alpha_1$, where E_{max} is the maximum energy that particle achieves (see eq. (22)). It is shown that E_{max} with extreme obliqueness is about 1500 times of that in parallel ($\eta = 1$). By using the proper assumption that η distributes uniformly and putting indices and absolute fluxes at 10^{12} eV for various elemental groups, we calculate spectra and composition of cosmic rays up to much higher energies. It is shown that $E_{\text{critical}} = 1.25 \times 10^{14} Z$ eV, where spectral curves start to bend and continue up to $E_{\text{max}}(\eta = \eta_{\text{min}}) \simeq 1500 \times E_{\text{critical}}$. These are well fitted with proton spectrum and explain a smooth knee behavior around 3×10^{15} eV.

We choose two parameter sets shown in Table 1. As to the total flux, “HEGRA” choice is fitted with DICE and CASA-MIA data, while “Ours” choice reproduces well Tibet γ and Akeno data up to several times 10^{17} eV. However, since our model is limited by E_{max} , in energies higher than $\sim 10^{17}$ eV, more energetic sources of cosmic rays should be necessary, such as pulsars and AGN where the outer magnetic fields are so strong. On the composition, our value of $\langle \ln A \rangle$ increases with the energy per particle as shown in Fig. 8. Data from various projects are scattered and have large uncertainties, particularly above E_{knee} . So the situation remains uncertain.

Here we neglect the dependence of power indices on obliqueness [35] and the quasi-perpendicular case where de-Hofmann-Teller frame cannot be used. These are problems remaining to be solved.

We are indebted T. Shibata at Aoyama Gakuin University for informing us new RUNJOB’s data before publication.

References

- [1] for example, M. Amenomori et al., *Astrophys. J.*, 461 (1996) 408.
- [2] for example, M. Nagano et al., *J. Phys. G10* (1984) 1295.
- [3] L. F. Fortson et al., *Proc. 26th Int. Cosmic Ray Conf. Vol. 3* (Salt Lake City, 1999) 125; J. W. Fowler et al., *astro-ph/0003190*.
- [4] R. Blanford, D. Eichler, *Phys. Rep.* 154 (1987) 1.
- [5] T. K. Gaisser, “Cosmic Rays and Particle Physics” (Cambridge University Press, 1990).
- [6] K. Kobayakawa, Y. Sato, T. Samura, *Proc. 26th Int. Cosmic Ray Conf., Vol. 4* (Salt Lake City, 1999) 467.
- [7] M. Ostrowski, *Mon. Not. R. astr. Soc.* 233 (1988) 257.
- [8] P. D. Hudson, *Mon. Not. R. astr. Soc.* 131 (1965) 23.
- [9] F. de Hoffmann, E. Teller, *Phys. Rev.* 80 (1950) 692.
- [10] L. O’ C. Drury, *Rep. Prog. Phys.* 46 (1983) 973.
- [11] F. Takahara, *Prog. Theor. Phys.* (1990) 83.
- [12] J. Nishimura et al., *Astrophys. J.* 238 (1980) 394.
- [13] P. O. Lagage, K. Cesarski, *Astrophys. J.* 118 (1983) 223.
- [14] E. G. Berezhko, *Astrop. Phys.* 5 (1997) 367.
- [15] A. M. Bykov, I. N. Toptygin, *Proc. 25th Int. Cosmic Ray Conf. Vol. 4* (Durban, 1997) 365.
- [16] E. G. Klepach et al., *Proc. 25th Int. Cosmic Ray Conf. Vol. 4* (Durban, 1997) 501.
- [17] P. L. Biermann, *Astron. Astrophys.* 271 (1993) 649.
- [18] M. M. Shapiro, M. Silberberg, *Ann. Rev. Nucl. Sci.* 20 (1970) 323.
- [19] F. Aharonian et al., *Phys. Rev. D* 59 (1999) 092003.
- [20] M. Amenomori et al., *Proc. 26th Int. Cosmic Ray Conf. Vol. 3* (Salt Lake City, 1999) 211.
- [21] M. Amenomori et al. (Tibet γ collaboration) submitted to *Phys. Rev. D* 2000.
- [22] JACEE collaboration, *Proc. 25th Int. Cosmic Ray Conf. Vol. 4* (Durban, 1997) 1; JACEE collaboration, *Astrophys. J.* 502 (1998) 278.
- [23] A. V. Apanasenko et al. (RUNJOB collaboration), submitted to *Astropar. Phys.* (2000).

- [24] K. Bernlöhr et al., *Astrop. Phys.* 8 (1998) 253.
- [25] T. Stanev, P. L. Biermann, T. K. Gaisser, *Astron. Astrophys.* 274 (1993) 902.
- [26] M. Nagano et al., *J. Phys.* G18 (1992) 423.
- [27] S. P. Swordy, D. B. Kieda, *Proc. 26th Int. Cosmic Ray Conf. Vol. 3* (Salt Lake City, 1999) 144; *Astrop. Phys.* 13 (2000) 137.
- [28] D. B. Kieda, S. P. Swordy, *Proc. 26th Int. Cosmic Ray Conf. Vol. 3* (Salt Lake City, 1999) 191.
- [29] M. A. K. Glasmacher et al., *Proc. 26th Int. Cosmic Ray Conf. Vol. 3* (Salt Lake City, 1999) 199.
- [30] A. Röhring et al., *Proc. 26th Int. Cosmic Ray Conf. Vol. 3* (Salt Lake City, 1999) 152.
- [31] A. A. Watson, *Proc. 25th Int. Cosmic Ray Conf. Vol. 8* (Durban, 1997) 257.
- [32] M. A. K. Glasmacher et al., *Proc. 26th Int. Cosmic Ray Conf. Vol. 3* (Salt Lake City, 1999) 129.
- [33] J. Engler et al., *Proc. 26th Int. Cosmic Ray Conf. Vol. 1* (Salt Lake City, 1999) 349.
- [34] C. Aguirre et al., ICRR-Report-460-2000-4(2000), Accepted in *Phys. Rev. D*.
- [35] T. Naito, F. Takahara, *Prog. Theor. Phys.* 93 (1995) 287.